Journal of Materials Chemistry B

ROYAL SOCIETY OF CHEMISTRY

PAPER

View Article Online
View Journal | View Issue

Cite this: J. Mater. Chem. B, 2022, 10, 7556

Biosafety evaluation of dual-responsive neutrobots

Hongyue Zhang,[ab] Liting Wang,[a] Zesheng Li,[a] Yuxing Ji,[c] Zhiguang Wu *[a] and Qiang He [ab]

Received 29th April 2022,
Accepted 8th June 2022

DOI: 10.1039/d2tb00938b

rsc.li/materials-b

The toxicity effects of paclitaxel (PTX)-loaded magnetic neutrophil-hybrid swimming microrobots ("neutrobots") *in vivo* were assessed after intravenous administration to mice. The mice after 72 hours exhibited minimal immunotoxicity and liver and kidney toxicity at an administration dose of 3×10^6 PTX-loaded neutrobots. The minor toxicity of drug-loaded neutrobots holds considerable promise for biomedical applications.

Introduction

Swimming micro/nanorobots as an innovative modality have attracted considerable attention due to their unprecedented features as well as promising potential, particularly in the areas of the active targeted delivery of therapeutic agents.[1–3] Swimming micro/nanorobots enable controllable propulsion in various fluids by the conversion of chemical or physical energy into mechanical motion.[4–8] Compared with conventional therapeutic micro/nanoparticles which rely on passive diffusion in biological fluids, swimming micro/nanorobots allow for the transportation of diverse therapeutic agents toward the hard-to-reach areas.[9,10] Among various swimming micro/nanorobots, magnetically actuated micro/nanorobots that are driven by an external magnetic field with uniform intensity have exhibited an impressive propulsion performance in various complex biological fluids ranging from blood flow to the vitreous of eyes.[11–13] With the efficient and precise mobility, the magnetic swimming micro/nanorobots are capable of conducting various tasks, including genome editing, non-invasive surgery, and environmental remediation.[14–19] However, the major magnetic swimming micro/nanorobots still have inherent limitations such as poor biocompatibility and biodegradability. With the rapid development in the field of biomedicine, swimming micro/nanorobots with biocompatible and biomimetic surfaces for favourable interfaces and interactions with natural biological subjects are urgently required.

To overcome these issues, diverse natural cell-hybrid magnetic swimming micro/nanorobots were developed in the past decade, and their movement behavior in biological fluids and biomedical applications has been investigated.[20] Sharing the unique biological functions of natural cells, diverse types of cells, such as red blood cells, macrophages, and neutrophils, have been utilized to develop swimming micro/nanorobots.[21,22] Particularly, neutrophil-hybrid magnetic swimming microrobots, namely neutrobots, have exhibited efficient magnetic propulsion and chemotaxis along the gradient of inflammatory factors for active therapy of glioma *in vivo*.[23] Although considerable progress has been accomplished on neutrobots, safety concerns are still remaining in its potential for immunogenicity and its relatively poor *in vivo* stability. There are no reports involving the safety evaluation of neutrobots *in vivo*.

[a] State Key Laboratory of Robotics and System, Harbin Institute of Technology, Harbin, 150001, China. E-mail: zhiguangwu@hit.edu.cn
[b] State Key Laboratory of Robotics, Shenyang Institute of Automation, Chinese Academy of Sciences, Shenyang, 110016, China
[c] School of Pharmaceutical Sciences, Guangzhou University of Chinese Medicine, Guangzhou, 510006, China

Zhiguang Wu

Zhiguang Wu is a Professor in the State Key Laboratory of Robotics and System, Harbin Institute of Technology. He earned his PhD in chemical engineering and technology from the Harbin Institute of Technology in 2015, and then he joined the Prof. Peer Fischer group at the Max Planck Institute for Intelligent Systems under an Alexander von Humboldt Foundation research fellowship. Subsequently, he continued his postdoctoral fellowship at the California Institute of Technology. His research interests are focused on the development of the next-generation of swimming micro/nanorobots for precision medicine. He is a recipient of the MIT Technology Review 35 Innovators under 35 in China list.

Here, we report the pharmacology and toxicity of the systematic administration of neutrobots in mice. To investigate the toxicological effect of drugs from neutrobots in the body, neutrobots were capsulated with paclitaxel (PTX) – a typical antitumor drug that also causes considerable side effects to normal tissues. According to a previous report, the PTX-loaded neutrobots by intravenous injection exhibited a remarkable therapeutic effect toward glioma *in vivo* upon the administration dose of 10^6 neutrobots per mouse.[23] The corresponding PTX dose from neutrobots is equivalent to that of the free PTX toward mice. Inheriting the biocompatibility and biodegradability of natural neutrophils, drug-loaded neutrobots are not susceptible to uptake by normal cells, accomplishing negligible toxicity *in vivo* which is essential to neutrobots for practical biomedical usages.

Materials and methods

Materials

Percoll was purchased from Biosharp Biotechnology Co., Ltd. $Fe(acac)_3$, gelatin, NaOH, hexanoic anhydride, 1,2-hexadecanediol, coumarin 6, dibenzyl ether, oleic acid, oleylamine, 1,1′-di-*n*-octadecyl-3,3,3′,3′-tetramethylindocarbocyanine perchlorate (DiI), Hoechst 33342, and 1,1-dioctadecyl-3,3,3,3-tetramethylindotricarbocyaine iodide (DiR) were purchased from Shanghai Yeasen Biotechnology Co., Ltd. Polycarbonate porous membranes (400 nm, 200 nm) were purchased from Whatman. Phosphotungstic acid was purchased from Beijing Solarbio Biotechnology Co., Ltd. RPMI 1640, DMEM, fetal blood serum (FBS), and PBS were purchased from Biosharp Biotechnology Co., Ltd. ELISA Kits (mouse TNF-α, IP-10, IFN-α, C3, IL-6, and histamine) were purchased from Shanghai Fanyin Biotechnology Co., Ltd.

Methods

Preparation and characterization

Preparation of EM@nanogels. EM@nanogels were fabricated *via* a camouflage process among *E. coli* outer membrane vesicles and nanometer scale gelatin particles, named nanogels. Nanogels were produced by dissolving amphiphilic gelatin and hydrophobic Fe_3O_4 nanoparticles[24] into the water–chloroform mixed dispersant, chloroform phase with 6 mg of paclitaxel (PTX) or without, and then the dispersant was heated to evaporate chloroform. Magnetic nanoparticles were prepared as described in the literature. The amphiphilic gelatin gathered on the interface between the water and chloroform, and, with chloroform evaporated, the gelatin aggregated around chloroform nanodroplets with Fe nanoparticles and eventually formed nanogel particles. The *E. coli* outer membrane vesicles were obtained by an ultracentrifugation method with 1 50 000 g for 2 h. Then, the nanogels and *E. coli* outer membrane vesicles were mixed and forced to pass through a polycarbonate membrane with a pore size of 200 nm under external pressure. After the extruding process, EM@nanogels were collected by 9800 g centrifugation 2 times.

Isolation of neutrophils. Neutrophils were collected from the murine bone marrow of KM or ICR mice. The RPMI 1640 medium was applied to flush the inner cavity of the mice tibia bone to obtain a bone marrow dispersion containing leukocytes, and then a discrete density gradient centrifugation means using the commercial Percoll mixture was applied to collect neutrophils from the interfaces of 71% and 61% volume fraction Percoll. More centrifugations would be applied to remove Percoll and red blood cells if necessary.

Preparation of neutrobots. For the preparation of neutrobots, the neutrophils were cultured with EM@nanogels for 30 min at 37 °C. EM@nanogels were phagocyted by neutrophils to form neutrobots. Excess EM@nanogels were separated by centrifugation.

TEM of neutrobots. Neutrobots were dehydrated step by step and dispersed in acetone. The resin was added to the acetone dispersion of neutrobots on a rotating shaking table. After the resin was cured, the sections were sliced and stained with uranyl acetate and lead citrate. Finally, the sectioned samples of neutrobots were observed by transmission electron microscopy H-7650 (Hitachi, Japan).

CLSM of neutrobots. Cou6 loaded EM@nanogels were used to prepare neutrobots. The nucleus of neutrobots was labelled by Hoechst 33342. DiI was used to label the cell membrane of neutrobots. The 3D images were captured and reconstructed using a Leica SP5 Confocal microscope.

Fe amount of neutrophils, neutrobots and neutrobots loaded with nanogels. The Fe amount was evaluated using ICP-AES.

Magnetic motion

Magnetic field setup. The magnetic field system contains a signal generator, a signal amplifier, a data acquisition card, Helmholtz coils, and a microscope. The magnetic field using in this experiment is the rotating magnetic field.

Trajectories and velocity of neutrobots. The movie of the motion of neutrobots was recorded. Trajectories of neutrobots were analyzed using ImageJ plugin Manual Tracker/Mtrack2. The velocity was calculated based on trajectories and motion time.

Plasma cytokine level test

KM mice (male, 6–8 weeks) were used in this experiment. The mice were intravenously injected with neutrobots loaded with PTX (3×10^6 cells per mouse). Before injection, a blood sample was collected as the control group (0 h). After scheduled times (12, 24, 48, and 72 h), blood samples were collected from the Kunming mice. The plasma was separated after centrifugation of the blood sample (3000 rpm, 30 min). ELISA kits were used to test plasma cytokine levels.

***In vivo* distribution of neutrobots.** KM mice (male, 6–8 weeks) were used in this experiment. Neutrobots (3×10^6 cells per mouse, labelled with DiR) were intravenously injected into mice. After injection, the mice were anesthetized by isoflurane. Then, the mice were imaged using the PERKINELMER IVIS Spectrum.

Liver function test and renal function test

A blood sample was collected from the KM mice injected with neutrobots (3×10^6 cells per mouse) after different time intervals. The tests were conducted by the laboratory department of the hospital of Harbin Institute of technology.

Pathological section of main organs after the injection of neutrobots. KM mice (male, 6–8 weeks) were used in this experiment. The mice were intravenously injected with neutrobots (3×10^6 cells per mouse). Before injection, a blood sample was collected as the control group (0 h). After scheduled times (12, 24, 48, and 72 h), the main organs (brain, heart, liver, spleen, lungs, and kidneys) were separated and fixed. The sections were stained with H&E, and the images were captured using OLYMPUS IX-73 inverted microscope with DP74 CCD camera.

All the animals were treated in accordance with the Guide for Care and Use of Laboratory Animals. Animal experiments were approved by the experimental animal welfare ethics committee of the Harbin Institute of technology (No. IACUC-2022032).

Results and discussion

Fabrication and characterization of neutrobots

The preparation of neutrobots contains three steps including the synthesis of gelatin-based nanogels, preparation of *E. coli* membrane-coated nanogels (EM@nanogels), and phagocytosis of EM@nanogels into neutrophils (Fig. 1A). Fe_3O_4 nanoparticles (Fe_3O_4 NPs) and PTX-loaded gelatin nanogels were fabricated utilizing an emulsion/solvent evaporation method as described in a previous report.[23] Furthermore, the *E. coli* membrane, acting as a multifunctional scaffold that prevents the intracellular release of PTX and activates neutrophils to engulf EM@nanogels, was fused onto the nanogel through co-extruding of the nanogel and *E. coli* membrane nanovesicles. The resulting neutrobots were obtained by the phagocytosis of EM@nanogels using neutrophils. To confirm the presence of EM@nanogels inside the neutrobots, coumarin 6 (Cou6)-labeled EM@nanogels were introduced into the fabrication process of neutrobots. The three dimensional confocal laser scanning microscopy image in Fig. 1B illustrated the green flourescence from Cou6 inside the neutrobots, indicating the successful incoporation of EM@nanogels toward neutrobots. Next, the ultrastructure analysis of neutrobots using ultramicrotomy was conducted to visualize the subcellular distribution of EM@nanogels. The ultrathin TEM section image of neutrobots in Fig. 1C displayed a significant number of EM@nanogels inside the neutrobots. The corresponding enlarged TEM image displayed that these particles were aggregated and encapsulated in an phagosome membrane inside the cytoplasm of neutrobots. Inductively coupled plasma/mass spectrometry (ICP-MS) analysis was conducted to further quantify the iron phagocytosis by the neutrobots. As shown in Fig. 1D, an up an uptake of 190.5 ng of iron per 1000 neutrobots was observed from the EM@nanogels, while the neutrobots that were prepared with bare nanogels rather than EM@nanogels had an uptake of 55.1 ng per 1000 cells. The near 4-fold elevation in the amount of iron clearly verifies that the coating of the *E. coli* membrane can effectively enhance the phagocytosis of EM@nanogels by neutrophils.

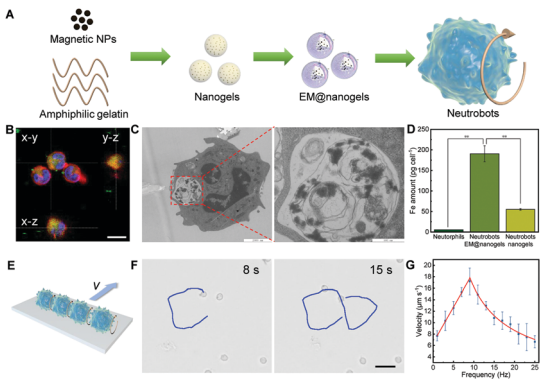

Fig. 1 Fabrication, characterization and magnetic propulsion of neutrobots. (A) Scheme of the preparation of neutrobots. (B) CLSM images of neutrobots (Cou6-EM@nanogels, Hoechst 33342-nucleus, and DiI-cell membrane). (C) TEM image of a neutrobot. Scale bar, 2 μm. The enlarged image shows EM@nanogels inside the neutrobot. Scale bar, 500 nm. (D) Fe amount of neutrophils, neutrobots and neutrobots with nanogels. ** $p < 0.01$. (E) Scheme of the magnetic motion of neutrobots under a rotating magnetic field. (F) Controlled motion of a single neutrobot under a magnetic field. (G) Motion velocity of single rolling neutrobots under RMF with different frequencies (15 mT).

The magnetically actuated propulsion of neutrobots upon application of an external rotating magnetic field with a uniform intensity is attributed to the interaction between neutrobots and the substrate (Fig. 1E). The capability of PTX-loaded neutrobots to efficiently locomote *in vitro* was first examined. The microscopic images in Fig. 1F illustrate the movement of neutrobots under the rotating magnetic field with a frequency of 30 Hz and an intensity of 15 mT in 15 s. The corner trajectory of neutrobots was achieved by the manipulation of the direction of the rotating magnetic field. Moreover, the velocity of neutrobots can be controlled by operating the frequency of the rotating magnetic field. As shown in Fig. 1G, the average velocity increases from 7.7 μm s^{-1} at 1 Hz to 17.2 μm s^{-1} at 9 Hz. It should be noted that the intensity of the employed rotating magnetic field plays a minor role in the toxicity toward normal cells.

Dynamic distribution of neutrobots *in vivo*

To investigate the safety profile of neutrobots *in vivo*, PTX-loaded neutrobots were injected through the caudal vein in a dose of 3×10^6 neutrobots per mouse according to a previous report.[23] Such a dose was comparable to the number of neutrophils in the whole mouse, and the dose cannot be elevated anymore. In this case, the distribution of injected neutrobots *in vivo* as a function of time was first studied. To visualize the dynamic distribution *in vivo*, the neutrobots were loaded with a DiR fluorescent dye. IVIS Spectrum *in vivo* imaging instruments were used to continuously characterize the change of the fluorescence intensity of mice in 60 min. As shown in Fig. 2, the real-time change of the fluorescence

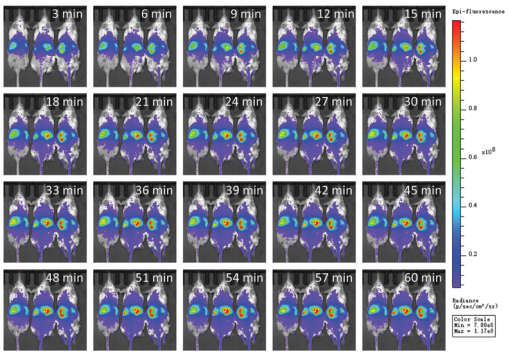

Fig. 2 *In vivo* distribution of neutrobots after injection into mice (3×10^6 cells per mouse) at different processing timescales. Scale bar, 10 mm.

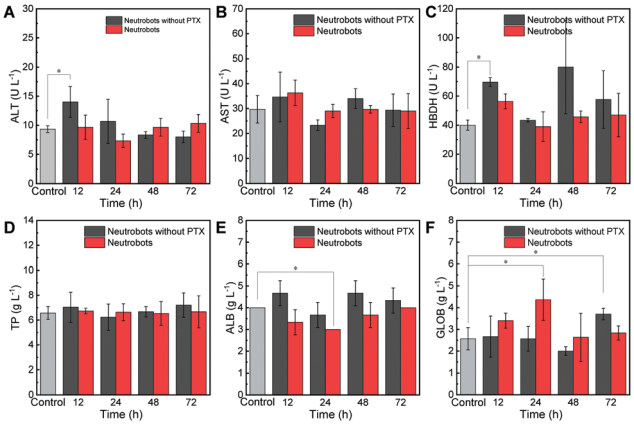

Fig. 3 Liver function tests of KM mice injected with neutrobots at specific time points after injection. Mice of the control group with no injection, and mice injected with 3×10^6 neutrobots loaded with PTX or not. (A) Serum alanine aminotransferase (ALT) concentration, (B) serum aspartate aminotransferase (AST) concentration, (C) serum α-hydroxybutyrate dehydrogenase (HBDH) concentration, (D) serum total protein (TP) concentration, (E) serum albumin (ALB) concentration, and (F) serum globulin (GLOB) concentration. $N = 3$, * $p < 0.05$.

intensity displayed that the fluorescence intensity in liver rapidly increased in first 30 min, consistent with the existing judgment that the liver is the main detoxification organ in mammals.[25] After that, there was negligible change in the fluorescence intensity of the mouse except the liver, the above changes could be obtained by reading the numerical changes of ROIs. These changes indicated that mice are metabolizing, and decomposing DiR injected into the body, implying that neutrobots can be excreted from the body through the normal metabolic pathway of mammals. The results shown in Fig. 2 prove that neutrobots had a normal metabolic pathway in mammals and did not affect the survival of mice in the experiment.

Effects of neutrobots toward liver *in vivo*

Next, the toxicity of neutrobots toward liver *in vivo* was studied by collecting the blood samples of mice injected with neutrobots to detect their liver functions. Alanine aminotransferase (ALT) and aspartate aminotransferase (AST) are important enzymes in the liver.[26] Evaluating the content of liver enzymes in the serum can evaluate liver injury and dysfunction. Mice without the injection of neutrobots were used as the control group. In the liver function test, Fig. 3A shows the serum ALT concentration test. Elevated ALT usually shows liver injury. After injecting neutrobots without PTX, the ALT concentration was 14 U L^{-1} at 12 hours, which increased briefly compared with the ALT concentration of the control group (9.3 U L^{-1}). At 24 hours, it decreased to 10.7 U L^{-1}, which has no significant diffenernce with the concentration of the control group.

At 48 hours and 72 hours, the ALT concentration was 8.3 and 8 U L^{-1} respectively, which was lower than the ALT concentration of the control group. After the injection of PTX-loaded neutrobots, the concentrations of ALT at 12, 24, 48 and 72 hours were 9.7, 7.3, 9.7 and 10.3 U L^{-1}, respectively, which have no significant difference with that in the control group. Moreover, the test of serum AST in Fig. 3B shows that the AST concentration in the control group was 29.7 U L^{-1}. After the injection of neutrobots without PTX, the concentration of AST slightly increased at 12 hours. The concentrations of AST in the PTX-free neutrobots and PTX-loaded neutrobots groups were 34.7 and 36.3 U L^{-1}, respectively, and, decreased at 24 hours, the concentrations of AST were 23.3 and 29 U L^{-1}, respectively. There was no significant change in the AST concentration at 48 hours and 72 hours. The AST test results showed that neutrobots had no obvious damage to the liver. Furthermore, α-hydroxybutyrate dehydrogenase (HBDH) is a kind of cell death marker. Acute hepatitis and heart and kidney injury may cause the increase of HBDH.[27] After the injection of neutrobots, HBDH in the PTX free neutrobots group and the PTX loaded neutrobots group increased slightly (Fig. 3C). Compared with the HBDH concentration in the control group (40 U L^{-1}), HBDH in the PTX free neutrobots group increased to 80 U L^{-1} at 48 hours and then decreased to 57.7 U L^{-1} at 72 hours. In the PTX loaded neutrobots group, HBDH reached 56.3 U L^{-1} at the highest and decreased rapidly after 12 hours. The results from 24 hours to 72 hours have no significant difference to those in the control group, indicating that a very short process of cell damage may be caused after the injection of neutrobots. There is a small fluctuation in the HBDH concentration, and it quickly returns to the normal range in a short time. In order to test the liver function, the contents of the serum total protein (TP), albumin (ALB) and globulin (GLOB) were measured at the same time. Fig. 3D shows that the TP after the injection of neutrobots is moderate and maintained in a stable range, which is similar to the value of the control group. The injection of neutrobots has no effect on the total serum protein. Fig. 3E shows that ALB fluctuated slightly after the injection of neutrobots. After the increase of ALB in the PTX free neutrobots group, it was maintained at a similar amount to that in the control group. After the injection of PTX loaded neutrobots, ALB decreased briefly and returned to a range similar to that of the control group at 48 hours. Fig. 3F shows that the GLOB concentration increased briefly after the injection of PTX loaded neutrobots, which

was 4.4 g L^{-1} at 24 hours, compared with 2.6 g L^{-1} in the control group, which may be due to the transient immune response. Then it rapidly decreased to 2.6 g L^{-1} at 48 hours, indicating that the injection of neutrophils had only a transient effect on the globulin content. Based on the above results, the effect of neutrobots injected into mice on liver function can be ignored and did not cause the increase of transaminase and drastic changes in the serum protein concentration, indicating that neutrobots have very little toxicity to the liver.

Toxicity evaluation of neutrobots toward kidney *in vivo*

Blood urea nitrogen (BUN) and serum creatinine (CREA) are markers of renal function[28] and UREA/CREA. The kidney is responsible for the drug metabolism and is vulnerable to damage. BUN may be affected by the protein intake and metabolic status. Fig. 4A shows the CREA concentration in blood, and there was no significant change in the content of creatinine, while the BUN value decreased slightly, which is shown in Fig. 4B. There may be many reasons for the decrease in BUN, except for the impaired renal function, so it can be considered that the renal function of the mice was not affected. Fig. 4C shows UREA/CREA values in blood, similar with BUN results, UREA/CREA values were decreasing. As an increased UREA/CREA indicates the impaired kidney function, the decreased result also has few things to do with the kidneys. Fig. 4D shows the blood glucose concentration, and all data were in a normal range. In summary, injected neutrobots are not toxic to the kidneys.

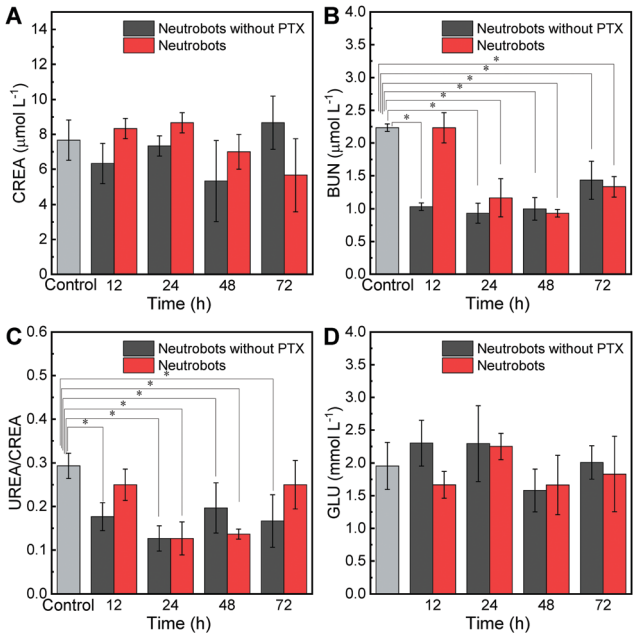

Fig. 4 Renal function tests of KM mice injected with neutrobots at specific time points after injection. Mice of the control group with no injection, and mice injected with 3 × 10^6 neutrobots loaded with PTX or not. (A) Serum creatinine (CREA) concentration, (B) blood urea nitrogen (BUN) concentration, (C) urea creatinine ratio (UREA/CREA), and (D) serum glucose (GLU) concentration. $N = 3$, * $p < 0.05$.

Evaluation of immunotoxicity caused by neutrobots *in vivo*

It is not only necessary to characterize the metabolism of neutrobots in mice, but also to analyze whether neutrobots will cause additional immune responses in mice, such as incremental immune rejection. Therefore, the following experiments were designed: the contents of various cytokines and immune factors in the mouse serum were detected within 72 hours after the injection of 3 × 10^6 neutrobots, to judge whether the injection of neutrobots caused an additional immune response. Six kinds of cytokines were tested; they were tumor necrosis factor-α (TNF-α), interferon g-inducible protein 10 (IP-10), IFN-α, complement components (C3), interleukin-6 (IL-6), and histamine.

The test results are shown in Fig. 5, indicating that the contents of six cytokines were within the normal range. TNF-α is used in the immune system for cell signaling. During an inflammatory response, macrophages or leukocytes release TNF-α as a communication between immune cells.[29] The stable TNF-α content indicated that the injection of neutrobots did not cause severe inflammation and subsequent cytokine release (Fig. 5A). IP-10, also known as the CXC motif chemokine ligand 10 (CXCL10), has chemical attraction to monocytes/macrophages, T cells, *etc.*, and promotes the adhesion of T cells to endothelial cells, antitumor activity and inhibition of bone marrow colony formation and angiogenesis.[30] After neutrobots were injected into mice, IP-10 was stable at 0–72 h, indicating that neutrobots had a negligible effect on the immune system and the fluctuation is very small (Fig. 5B). IFN-α is a type I interferon, which plays an important role in inflammation, immune regulation, and other reactions and has anti-tumor activity.[31] After neutrobots were injected into the body, IFN-α shows a slightly down-regulation at 0 to 24 h, from 20.7 to 15.5 pg mL^{-1}, and then return to 21.8 pg mL^{-1} at 48 h (Fig. 5C). IFN-α shows a stable level after the injection. Complement component 3 (C3) plays a key role in the complement system

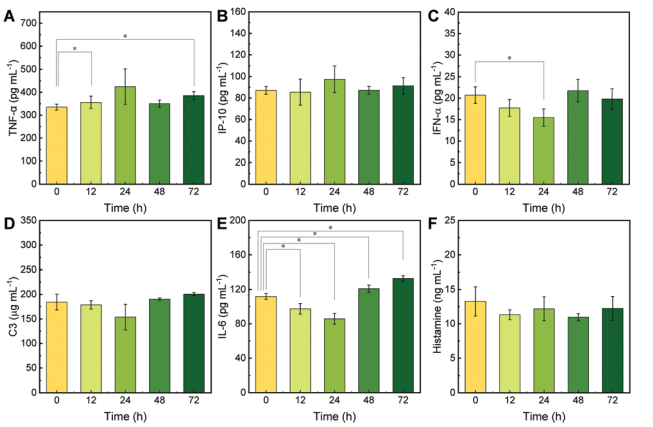

Fig. 5 Plasma cytokine levels in mice after injection with neutrobots loaded with PTX (3 × 10^6 cells per mouse) and different processing timescales. (A) Tumor necrosis factor-α (TNF-α) levels, (B) interferon g-inducible protein 10 (IP-10) levels, (C) IFN-α levels, (D) complement component (C3) levels, (E) interleukin-6 (IL-6) levels, and (F) histamine levels; $N = 3$, * $p < 0.05$.

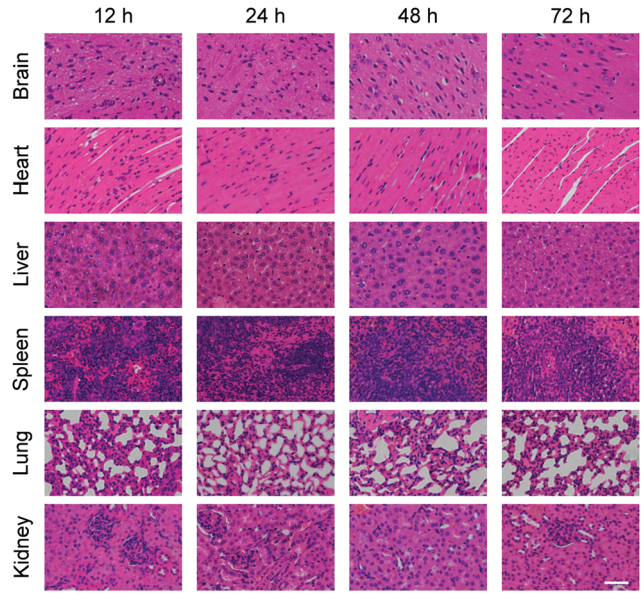

Fig. 6 Pathological section of main organs (brain, heart, liver, spleen, lungs and kidneys) separated from mice after injection with PTX free neutrobots and different processing timescales. Scale bar, 50 μm.

and is conducive to innate immunity. The C3 elevation is common in the early stage of acute inflammation.[32] After injection into the mice, the small fluctuation of C3 caused by neutrobots indicates that the impact time of neutrobots on the internal environment is short and can return to normal after 72 hours (Fig. 5D). Interleukin-6 (IL-6) can be used as a proinflammatory factor and anti-inflammatory factor. As an inflammatory marker, IL-6 is an important mediator of the acute inflammatory response.[33] After the injection of neutrobots into the mice, the concentration of IL-6 decreased slightly, and gradually returned to a slightly higher level, which may be due to the early weak inflammation caused by many neutrobots (Fig. 5E). Histamine is a central neurotransmitter involved in inflammatory responses and increases capillary permeability.[34] It can promote the entry of neutrobots into tissues and provide conditions for neutrobots to function. Histamine keeps a stable level from 0 to 72 h (Fig. 5F). A variety of cytokine tests showed that the injection of neutrobots did not cause significant fluctuations of cytokines *in vivo*. After the injection of neutrobots, the cytokines in the mouse serum remained stable. The above results show that the injection of neutrobots does not cause serious side effects such as inflammation or an inflammatory factor storm, and it is safe as an injection.

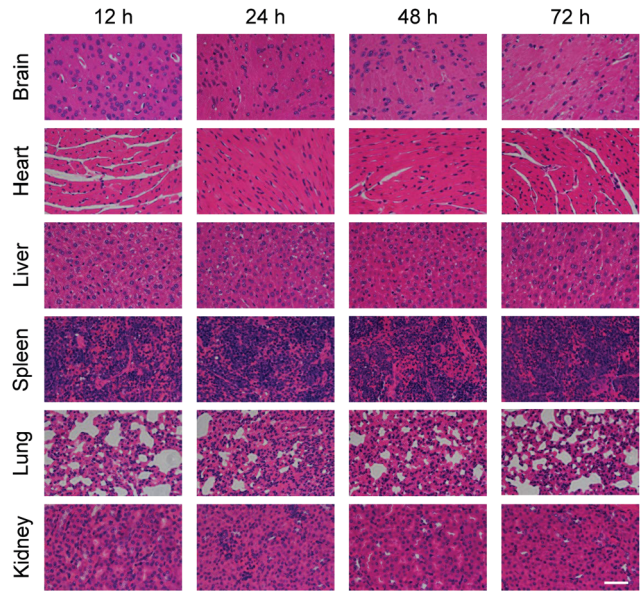

Fig. 7 Pathological section of main organs (brain, heart, liver, spleen, lungs and kidneys) separated from mice after injection with neutrobots loaded with PTX and different processing timescales. Scale bar, 50 μm.

Besides the concentration test of cytokines, pathological sections were made for the organs obtained after the dissection of mice in each experimental group. The results are shown in Fig. 6 and 7. Fig. 6 shows the pathological sections of mice injected with neutrobots without PTX. Fig. 7 shows the pathological sections of mice injected with neutrobots loaded with PTX. The optical microscope photographs of the pathological sections of six main organs showed that the morphology of each organ of the experimental group was normal and was not damaged by neutrobots.

No differences were observed between pathological sections collected from mice injected with neutrobots with PTX (Fig. 7) and without PTX (Fig. 6). In summary, the injection of neutrobots into mice would not cause additional immune rejection, would not damage the normal tissues and organs of mice, and could be excreted along the general metabolic pathway. It should be noted that the toxicity evaluation of PTX-loaded neutrobots *in vivo* was conducted in healthy mice according to previous reports,[35,36] the minor effect on the tissue histopathology, activity of liver, kidney, and immunity, suggesting that the treatment of PTX-loaded neutrobots is safe in the mouse model. More in-depth studies for the evaluation of neutrobots including the toxicity profile with an expanded period *in vivo*, metabolic pathway, and molecular mechanism will be carried out in future research.

Conclusions

In conclusion, the toxicological properties of PTX-loaded neutrobots adminstered by injection were evaluated for 72 hours upon the administration dose of 3×10^6 neutrobots per mouse according to a previous report. Compared with the widely acknowledged toxicity of PTX to the body, the data indicate that the delivery of PTX using neutrobots caused minor effects on the functions of the immune system, liver, and kidney. Although these investigations were not carried out to support the advancement of clinical candidates, they reflected that the neutrobots might be feasible for the safe delivery of therapeutic levels of the drug. Future studies will focus on the dynamic pharmacology, pharmacokinetics of various drug-loaded

neutrobots with repeated administration, and the risk for juvenile animals.

Funding

This work was financially supported by the National Natural Science Foundation of China (grant no. 21972035 and 22002020), the Interdisciplinary Research Foundation of HIT (grant no. IR2021112), and the State Key Laboratory of Robotics (grant no. 2019-O02).

Author contributions

Z. W. conceived the project. Z. W. supervised the studies. H. Z. and Z. L. prepared and characterized the neutrobots. H. Z. and L. Z. performed the magnetic movement experiments. H. Z. and Y. J. drew the schematic illustrations. H. Z. and L. W. conducted the *in vivo* experiments. Z. W. and H. Z. interpreted data and wrote the manuscript. All the authors reviewed the manuscript.

Conflicts of interest

There are no conflicts to declare.

Notes and references

1 W. Gao, R. Dong, S. Thamphiwatana, J. Li, W. Gao, L. Zhang and J. Wang, *ACS Nano*, 2015, **9**, 117–123.
2 J. Li, B. Esteban-Fernández de Ávila, W. Gao, L. Zhang and J. Wang, *Sci. Robot.*, 2017, **2**, eaam6431.
3 M. Sitti, *Nat. Rev. Mater.*, 2018, **3**, 74–75.
4 T. Xu, W. Gao, L.-P. Xu, X. Zhang and S. Wang, *Adv. Mater.*, 2017, **29**, 1603250.
5 T. Xu, F. Soto, W. Gao, R. Dong, V. Garcia-Gradilla, E. Magaña, X. Zhang and J. Wang, *J. Am. Chem. Soc.*, 2015, **137**, 2163–2166.
6 R. Dong, Y. Cai, Y. Yang, W. Gao and B. Ren, *Acc. Chem. Res.*, 2018, **51**, 1940–1947.
7 R. Dong, Y. Hu, Y. Wu, W. Gao, B. Ren, Q. Wang and Y. Cai, *J. Am. Chem. Soc.*, 2017, **139**, 1722–1725.
8 F. Mou, Q. Xie, J. Liu, S. Che, L. Bahmane, M. You and J. Guan, *Natl. Sci. Rev.*, 2021, **8**, nwab066.
9 M. Wan, H. Chen, Q. Wang, Q. Niu, P. Xu, Y. Yu, T. Zhu, C. Mao and J. Shen, *Nat. Commun.*, 2019, **10**, 966.
10 M. Zhou, Y. Xing, X. Li, X. Du, T. Xu and X. Zhang, *Small*, 2020, **16**, 2003834.
11 J. Yu, D. Jin, K.-F. Chan, Q. Wang, K. Yuan and L. Zhang, *Nat. Commun.*, 2019, **10**, 5631.
12 X. Yang, W. Shang, H. Lu, Y. Liu, L. Yang, R. Tan, X. Wu and Y. Shen, *Sci. Robot.*, 2020, **5**, eabc8191.
13 J. Liu, S. Yu, B. Xu, Z. Tian, H. Zhang, K. Liu, X. Shi, Z. Zhao, C. Liu, X. Lin, G. Huang, A. A. Solovev, J. Cui, T. Li and Y. Mei, *Appl. Mater. Today*, 2021, **25**, 101237.
14 H. Wang and M. Pumera, *Chem. Rev.*, 2015, **115**, 8704–8735.
15 F. Mou, X. Li, Q. Xie, J. Zhang, K. Xiong, L. Xu and J. Guan, *ACS Nano*, 2020, **14**, 406–414.
16 T. Yu, A. G. Athanassiadis, M. N. Popescu, V. Chikkadi, A. Güth, D. P. Singh, T. Qiu and P. Fischer, *ACS Nano*, 2020, **14**, 13673–13680.
17 M. Li, X. Wang, B. Dong and M. Sitti, *Nat. Commun.*, 2020, **11**, 3988.
18 M. Pacheco, B. Jurado-Sánchez and A. Escarpa, *Angew. Chem., Int. Ed.*, 2019, **58**, 18017–18024.
19 K. Yuan, B. Jurado-Sánchez and A. Escarpa, *Angew. Chem., Int. Ed.*, 2021, **60**, 4915–4924.
20 B. Esteban-Fernández de Ávila, W. Gao, E. Karshalev, L. Zhang and J. Wang, *Acc. Chem. Res.*, 2018, **51**, 1901–1910.
21 F. Zhang, R. Mundaca-Uribe, H. Gong, B. Esteban-Fernández de Ávila, M. Beltrán-Gastélum, E. Karshalev, A. Nourhani, Y. Tong, B. Nguyen, M. Gallot, Y. Zhang, L. Zhang and J. Wang, *Adv. Mater.*, 2019, **31**, 1901828.
22 Y. Dai, X. Bai, L. Jia, H. Sun, Y. Feng, L. Wang, C. Zhang, Y. Chen, Y. Ji, D. Zhang, H. Chen and L. Feng, *Small*, 2021, **17**, 2103986.
23 H. Zhang, Z. Li, C. Gao, X. Fan, Y. Pang, T. Li, Z. Wu, H. Xie and Q. He, *Sci. Robot.*, 2021, **6**, eaaz9519.
24 S. Sun, H. Zeng, D. B. Robinson, S. Raoux, P. M. Rice, S. X. Wang and G. Li, *J. Am. Chem. Soc.*, 2004, **126**, 273–279.
25 F. Zaefarian, M. R. Abdollahi, A. Cowieson and V. Ravindran, *Animals*, 2019, **9**, 63.
26 R. J. Church and P. B. Watkins, *J. Dig. Dis.*, 2019, **20**, 2–10.
27 A. Zinellu, P. Paliogiannis, C. Carru and A. A. Mangoni, *Clin. Exp. Med.*, 2021, DOI: **10.1007/s10238-021-00777-x**.
28 B. R. Griffin, S. Faubel and C. L. Edelstein, *Ther. Drug Monit.*, 2019, **41**, 213–226.
29 J. A. Baugh and R. Bucala, *Curr. Opin. Drug Discovery Dev.*, 2001, **4**, 635–650.
30 P. Romagnani and C. Crescioli, *Clin. Chim. Acta*, 2012, **413**, 1364–1373.
31 S. Pasquali and S. Mocellin, *Curr. Med. Chem.*, 2010, **17**, 3327–3336.
32 J. R. Delanghe, R. Speeckaert and M. M. Speeckaert, *Pathology*, 2014, **46**, 1–10.
33 M. Mihara, M. Hashizume, H. Yoshida, M. Suzuki and M. Shiina, *Clin. Sci.*, 2011, **122**, 143–159.
34 L. Maintz and N. Novak, *Am. J. Clin. Nutr.*, 2007, **85**, 1185–1196.
35 B. E.-F. De Ávila, P. Angsantikul, J. Li, M. Angel Lopez-Ramirez, D. E. Ramírez-Herrera, S. Thamphiwatana, C. Chen, J. Delezuk, R. Samakapiruk, V. Ramez, M. Obonyo, L. Zhang and J. Wang, *Nat. Commun.*, 2017, **8**, 272.
36 M. Wan, Q. Wang, R. Wang, R. Wu, T. Li, D. Fang, Y. Huang, Y. Yu, L. Fang, X. Wang, Y. Zhang, Z. Miao, B. Zhao, F. Wang, C. Mao, Q. Jiang, X. Xu and D. Shi, *Sci. Adv.*, 2020, **6**, eaaz9014.

